



# GRiD MT (grid-based real-time determination of moment tensors) monitoring the long-period seismic wavefield

Hiroshi Tsuruoka\*, Hitoshi Kawakatsu, Taku Urabe

*The Earthquake Research Institute, The University of Tokyo 1-1-1 Yayoi, Bunkyo-ku, Tokyo 113-0032, Japan*

## ARTICLE INFO

### Article history:

Received 20 August 2007

Accepted 29 February 2008

### PACS:

91.30.Bi

### Keywords:

Seismic sources

Automated real-time system

Moment tensor inversion

## ABSTRACT

We have developed and implemented a new grid-based earthquake analysis system that continuously monitors long-period seismic wavefield of 20–50 s recorded by broadband seismometers. The new analysis system automatically and simultaneously determines the origin time, location and seismic moment tensor of seismic events within 3 min of their occurrence. This system has been in operation since 2003 at the Earthquake Research Institute (<http://www.eri.u-tokyo.ac.jp/GRiD MT/>), and the locations and origin times are usually obtained within 3 s and 20 km away from the earthquake catalog values determined by the Japan Meteorological Agency (JMA). In addition, moment tensor solutions are comparable to the network solutions manually obtained. This new system should enable us to monitor long-period seismic wavefield continuously further to help identifying long-period (or low-frequency) events which are undetectable by the conventional monitoring of short-period seismic wavefields.

© 2009 Elsevier B.V. All rights reserved.

## 1. Introduction

Until now, many automated waveform data processing systems have been developed that use waveform inversion techniques to determine earthquake source mechanisms (i.e., CMT solutions). For earthquakes with moment magnitude larger than 5, moment tensors are routinely determined by several institutes using long-period waveforms observed by the worldwide seismic networks (Dziewonski et al., 1981; Sipkin, 1994; Kawakatsu, 1995).

For regional earthquakes, there are several attempts to estimate moment tensors using regional broadband networks. For example, Thio and Kanamori (1995) analyzed moment tensors of local earthquakes using TERRA-scope regional broadband surface waveforms. Dreger and Helmberger (1993) developed a broadband body wave inversion to estimate regional earthquakes using three-component sparse network data. Moment tensor of regional earthquakes in various countries and areas are now determined using this algorithm. In Japan, using the Japanese regional broadband seismic network (called F-net) Fukuyama et al. (1998) determined routinely moment tensors of small earthquakes ( $M > 3.5$ ). Bernardi et al. (2004) determined moment tensor of earthquakes occurred in the European-Mediterranean region.

As all of these systems are started after receiving information about earthquake occurrences, they basically process data that is already saved on hard disks, rather than a real-time data flow of waveforms. For this reason, it is difficult to reduce the time lag between the earthquake occurrence and the determination of the earthquake mechanism, as these solution systems must wait until they receive information concerning the earthquake's origin time and location.

To circumvent this situation, Kawakatsu (1998) suggested a possibility of monitoring the long-period wavefield in real-time using a grid-based search algorithm. Tajima et al. (2002) have applied this approach to Berkeley Digital Seismic Network (BDSN) data with a  $0.25^\circ$  mesh of grid points. Recently, Ito et al. (2006, 2007) employed a similar technique that lead them to report very-low-frequency earthquakes occurring in the transition zone of the subducting plate interface along the Nankai subduction zone in southwest Japan. Auger et al. (2006) presented a comprehensive processing tool for the real-time analysis of moment tensors to monitor very long-period activity of the Stromboli volcano using a 62-node Linux cluster. Although these approaches do not use prior earthquake information, they use the waveform data stored on hard disks, rather than the actual real-time flow of data.

In this study, we introduce a new analysis system that uses waveform data in memory and distributed over a computer network to continuously monitor the long-period seismic wavefield. Kanamori et al. (1999) pointed out that such a continuous monitoring of waveforms enhances the reliability of the system because of minimization of the workload.

\* Corresponding author.

E-mail address: [tsuru@eri.u-tokyo.ac.jp](mailto:tsuru@eri.u-tokyo.ac.jp) (H. Tsuruoka).

## 2. Method

### 2.1. Inversion algorithm

A moment tensor inversion is considered for cases where the origin time and the source location are given. The observation equation of such an inversion is provided below, with  $s$  denoting the source and  $k$  the station:

$$G_i^{sk}(t)m_i^s = d^k(t) \quad (1)$$

where  $G_i^{sk}(t)$  is the theoretical waveform (Green's function) for  $i$ th component of the moment tensor, and  $d^k(t)$  the observed waveform, and the summation convention is assumed for subscripts. This equation is generalized for the three components of ground motion at station  $k$ .  $m_i^s$  refers to the  $i$ th component of the moment tensor at a source  $s$ . The corresponding normal equation is:

$$A_{ji}^s m_i^s = b_j^s \quad (2)$$

where  $A_{ji}^s = \sum_k A_{ji}^{sk}$ ,  $b_j^s = \sum_k b_j^{sk}$ ,  $A_{ji}^{sk} = \int G_j^{sk}(t)G_i^{sk}(t)dt$ , and  $b_j^{sk} = \int G_j^{sk}(t)d^k(t)dt$ . Hereafter, the superscript for the source,  $s$ , is omitted from equations when not confusing. The least squares solution of the moment tensor is then given by:

$$\hat{\mathbf{m}} = \mathbf{A}^{-1} \mathbf{b} \quad (3)$$

In this equation,  $\mathbf{A}$  is given once a structural model is specified as it can be provided solely by the Green's functions. So, we precompute the  $\mathbf{A}$  matrix and therefore  $\mathbf{A}^{-1}$  for each source-station pair. The inversion solution can therefore be obtained if  $\mathbf{b}$  can be estimated from the Green's function and the observed waveform. This shows that the procedure for estimating a moment tensor when a source location is given is almost equivalent with the calculating the cross-correlation between Green's functions and data. That is the most time-consuming processing. In addition, the prediction error of the observed waveforms for the obtained moment tensor is also easily calculated:

$$res = \left( \sum_k \int d^k(t)^2 dt \right) - \mathbf{b}^t \mathbf{A}^{-1} \mathbf{b} \quad (4)$$

Thus, for a given "virtual" source  $s$ , both the moment tensor (3) and the residual (4) can be easily estimated. This allows us to perform a grid-search type approach to find a moment tensor solution and a location of a virtual source which is most consistent (i.e., gives the least prediction error) with the observed wavefield. Kawakatsu (1998) suggested the possibility to do such a grid-search in real-time every 1 s to monitor the regional long-period seismic wavefield.

To search for the best solution, in the present approach, instead of the quantity estimated in (4), a variance reduction (VR)

$$VR = \left[ \frac{1 - res}{\sum_k \int (d^k(t))^2 dt} \right] \times 100(\%) \quad (5)$$

has been used in the actual monitoring. VR is an indicator of the fit between the observed waveform and the theoretical waveform.

### 2.2. Real-time analysis system

#### 2.2.1. Outline of the system

Our system consists of programs that perform the following tasks: (1) receiving of data (recvt, order), (2) filtering and conversion of data from the shared memory into the standard output (shmdump), (3) moment tensor inversion (rmtinv), (4) detection of an earthquake (EventDetect.pl), (5) visualization (mtplot, shmx, mtx) and dissemination programs (e-mailing, www). All these programs work together to form the complete system. Programs (1) and (2) were prepared using those from the WIN system (Urabe, 1994). The WIN system continuously collects and distributes real-time waveform data among nation-wide stations and data centers in Japan. The WIN format, which is based on time-stamped variable-length data packets, is used for both transmission and storage of waveform data. This system also has various processing package, such as the hypocenter determination and the picking of P and S arrivals. Programs (3)–(5) were developed in the current study. Since all of these programs have been developed for clearly defined modular functionality, the system is capable of flexibly accommodating changes and modifications. Fig. 1 shows how these programs are interrelated. The programs have also been developed to facilitate offline processing of data as well as real-time processing.

#### 2.2.2. System configuration

As this earthquake analysis system requires a high level of computational performance and computers with large memory resources, we used PCs with the specifications shown below for the actual monitoring: CPU: Intel Xeon 3.06 GHz; Memory: 1 GB PC2100 DDR SDRAM. For both the system and memory, bandwidth is 4.2 GB/s. A system with insufficient memory bandwidth, such as a Pentium III (1.06 GB/s), is not capable of real-time processing. Each of the PCs is connected to a broadcast segment to which data from the satellite or terrestrial is distributed, so the PCs can easily share seismic waveform data.

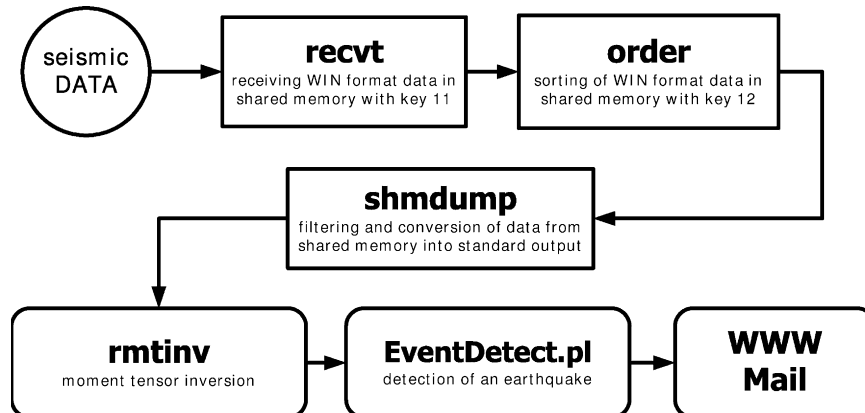


Fig. 1. Outline of the real-time earthquake analysis system used in this study.

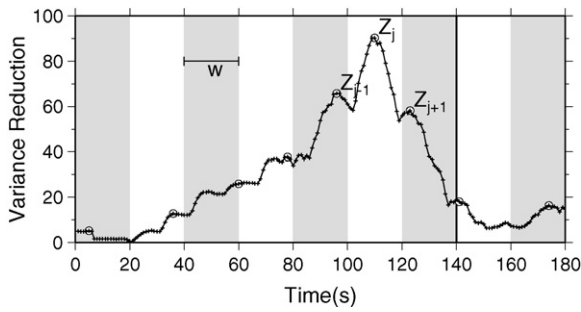


Fig. 2. Earthquake detection algorithm. An event is detected at 140 (s) in this case.

2.3. Monitoring details

2.3.1. Period range

In ordinary moment tensor inversions, the frequency band used for analysis may be modified to adjust for the earthquake magnitude. Our system, however, employs a fixed frequency band because it performs continuous real-time processing. Considering the degree of seismic activity in the monitored area, long-period wavefields of 20–50 s are used in this study. A recursive digital filter (Saito, 1978) is used as the band-pass filter for the waveform, as such a digital filter works well with real-time processing. The broadband seismometers installed at Japanese stations produce velocity

Table 1  
Velocity structure used for Green's function.

Thickness (km)	P velocity (km/s)	S velocity (km/s)	Density (kg/m <sup>3</sup> )	Q <sub>p</sub>	Q <sub>s</sub>
3	5.5	3.14	2300	600	300
15	6.0	3.55	2400	600	300
15	6.7	3.83	2800	600	300
67	7.8	4.46	3200	600	300
∞	8.0	4.57	3300	600	300

records, which are used directly to reduce processing time rather than integrating to displacement as commonly done.

2.3.2. Record length, station number and grid size

The record length, number of stations, and number of virtual sources need to be set in such a way that enables real-time processing. Considering that F-net determines a solution at three stations close to the hypocenter (Fukuyama et al., 1998), it is considered herein that the monitoring area is where real-time processing is possible at three stations. For a seismic wave that travels 400 km distance, P, S, surface, and other major waves arrive at stations within 2 min. For this reason, the record length used by the analysis is set for 2 min. As re-sampling of data is performed every second, the system collects 120 data points in total. As we used long-period waveforms (20–50 s), there is no need for high resolution in determining the hypocenter. Thus, virtual sources are

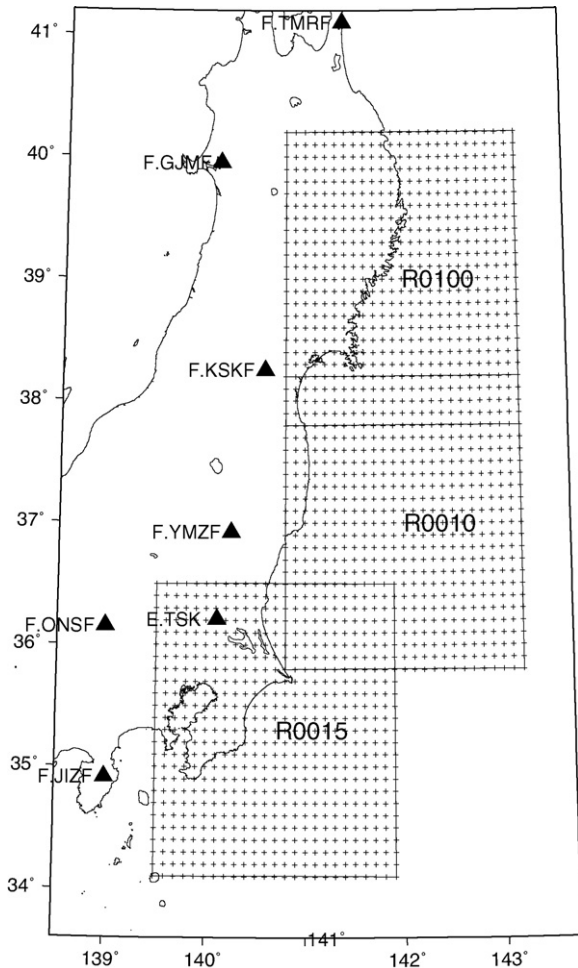


Fig. 3. Locations of stations (filled triangle) and virtual sources (plus). Three monitoring regions (R0010, R0015, R0100) are shown.

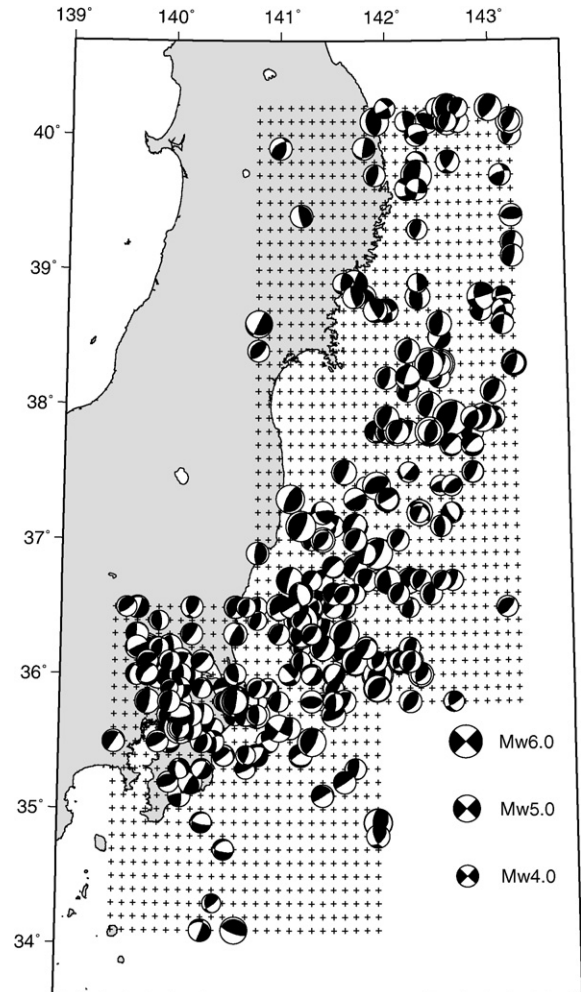


Fig. 4. Monitoring results from January 2004 to December 2006. The focal mechanisms are lower hemisphere projection and are scale by the moment magnitude.

located every  $0.1^\circ$  horizontally and every 9 km vertically (depth), which are both significantly less than the minimum wave length of the data used. Under these conditions, our tests show that real-time data processing is possible for up to approximately 7000 virtual sources. A single PC is therefore able to cover an area of  $2.4^\circ \times 2.4^\circ \times 90$  km ( $= 25 \times 25 \times 11 = 6875$  virtual sources,) in maximum. However improved computer performance in the future will enable more than three stations to be used for monitoring or more than 7000 virtual sources to be processed.

#### 2.4. Earthquake detection algorithm

As this system does not depend on a preliminary report of the seismic event occurrence, the system itself is required to detect the earthquake. The system monitors the VR of every  $\hat{m}^s$  which is determined every second, but the actual event detection is issued based on the maximum value of VRs for specified time windows whose length is  $w$  (Fig. 2). If the maximum value of VR within a specified time window ( $Z_j$  for  $j$ th time window) is larger than both those of the previous time window ( $Z_{j-1}$ ) and the next time window ( $Z_{j+1}$ ), then an event is detected; i.e., in a case where  $Z_j$  meets the condition below, this system decides that an earthquake has occurred:

$$Z_{j-1} \leq Z_j \geq Z_{j+1}, \quad Z_j \geq VR_0 \quad (6)$$

where  $VR_0$  is the event detection threshold, which is set to 65.0. Fig. 2 shows how an earthquake is detected. As  $w$  is set to 20 s, the

system recognizes an earthquake occurrence on average 30 s after VR takes a maximum value.

### 3. GRiD MT

We have implemented the real-time monitoring system based on the procedures described above to monitor the seismicity of the Pacific Ocean side of the northeast Japan, and have been operating the system since April 2003. The analysis system is termed GRiD MT (grid-based real-time determination of moment tensors), and real-time solutions have been available at the following URL: <http://www.eri.u-tokyo.ac.jp/GRiD-MT/>. As the web site displays 5 areas monitored, we discussed 3 areas monitored in this paper. Because we do real-time monitoring with fixed three stations, but the other 2 areas is unstable in waveform data acquisition with fixed three stations from 2004 to 2006.

#### 3.1. Monitoring area

All the broadband stations used in the present study are shown in Fig. 3. All the data is collected and distributed in real-time using a satellite telemetry system (Takano et al., 2001), which was recently changed to a terrestrial telemetry system. In terms of the area to be monitored, there is a restriction on the number of virtual sources that enables computation of (3) and (5) within a period of 1 s. Three different monitoring areas are defined, each containing  $25 \times 25 \times 11 = 6875$  virtual sources, as shown in Fig. 3. In the

**Table 2**  
Detected event list larger than  $M_w = 5.0$ .

No.	Origin time	LON	LAT	DEP	MAG	Mechanism	VR
1	2004/01/23,18:01:33	141.1000	37.3000	59.0	5.2	(206,69,87)	91.81
2	2004/02/04,15:08:27	141.9000	40.1000	68.0	5.2	(356,49,90)	85.13
3	2004/03/11,11:34:56	141.2000	36.3000	41.0	5.3	(15,68,79)	90.69
4	2004/04/04,08:01:59	141.4000	36.3000	41.0	5.9	(28,71,92)	91.41
5	2004/08/10,15:13:29	142.3000	39.7000	50.0	5.6	(15,74,98)	91.45
6	2004/08/21,05:33:02	141.9000	34.9000	23.0	5.3	(173,62,60)	72.62
7	2004/08/21,06:19:54	141.9000	34.9000	23.0	5.1	(180,58,67)	70.51
8	2004/09/01,11:49:27	141.9000	36.9000	41.0	5.7	(29,69,93)	90.75
9	2004/10/06,23:40:44	140.0000	36.1000	59.0	5.6	(4,67,88)	75.30
10	2004/10/17,02:19:17	141.7000	36.1000	32.0	5.4	(26,55,85)	89.51
11	2004/10/17,03:54:42	141.6000	36.2000	32.0	5.7	(31,63,91)	90.78
12	2004/11/02,22:04:24	142.9000	38.8000	5.0	5.1	(74,88,141)	86.13
13	2004/12/19,14:22:45	141.8000	36.1000	32.0	5.1	(34,56,97)	89.83
14	2004/12/29,22:58:45	142.5000	38.3000	41.0	5.6	(15,67,90)	95.17
15	2005/01/01,05:13:47	141.1000	36.7000	95.0	5.0	(195,81,-87)	79.32
16	2005/02/16,04:46:37	139.9000	36.0000	50.0	5.3	(37,73,77)	78.12
17	2005/04/04,02:57:09	141.9000	37.4000	41.0	5.1	(64,50,95)	87.90
18	2005/04/11,07:22:20	140.6000	35.8000	50.0	5.9	(5,77,95)	79.96
19	2005/05/27,17:07:22	140.8000	38.6000	86.0	5.0	(206,88,70)	87.01
20	2005/06/20,01:15:20	140.6000	35.8000	50.0	5.6	(16,77,93)	78.53
21	2005/07/23,16:35:00	140.1000	35.6000	59.0	5.8	(15,62,102)	76.27
22	2005/08/08,00:06:45	141.6000	36.3000	32.0	5.4	(26,60,90)	91.31
23	2005/10/12,13:30:12	142.1000	37.8000	41.0	5.1	(21,68,89)	95.25
24	2005/10/19,20:44:44	141.2000	36.4000	41.0	6.2	(29,74,99)	90.33
25	2005/10/22,22:12:47	141.2000	37.1000	50.0	5.5	(24,72,86)	92.52
26	2005/10/24,18:34:48	142.5000	38.3000	41.0	5.0	(13,63,86)	94.26
27	2005/12/02,22:13:05	142.6000	37.9000	41.0	6.5	(20,68,88)	95.05
28	2005/12/05,03:03:12	143.0000	40.2000	41.0	5.0	(37,66,105)	93.44
29	2005/12/05,07:20:20	142.9000	37.9000	32.0	5.2	(30,50,98)	91.69
30	2005/12/17,03:32:13	142.4000	38.3000	41.0	6.0	(12,66,86)	94.29
31	2006/01/18,23:25:23	142.4000	37.8000	23.0	5.4	(209,66,100)	82.66
32	2006/02/01,20:35:54	140.1000	35.7000	86.0	5.0	(231,83,-14)	76.75
33	2006/02/03,13:37:33	141.9000	36.0000	32.0	5.8	(25,51,85)	87.82
34	2006/02/03,15:10:02	141.9000	36.0000	32.0	5.3	(23,49,80)	87.71
35	2006/03/12,07:06:43	142.6000	40.1000	41.0	5.0	(26,74,92)	93.82
36	2006/03/13,13:06:10	141.9000	35.9000	32.0	5.1	(33,53,90)	85.89
37	2006/03/13,13:15:31	141.9000	35.9000	32.0	5.0	(32,50,89)	86.76
38	2006/07/01,08:28:09	142.4000	38.3000	41.0	5.2	(11,64,85)	94.47
39	2006/07/06,02:08:39	142.6000	40.2000	41.0	5.2	(26,71,101)	93.07
40	2006/09/07,03:06:30	141.3000	35.5000	50.0	5.2	(27,71,97)	77.83

actual monitoring, small parts of these three areas are overlapped. The details of each area are given below:

- R0010: 140.8–143.2E, 35.8–38.2N, 5–95 km depth (stations used: N.KSKF, N.YMZF, E.TSK)
- R0015: 139.5–141.9E, 34.1–36.5N, 5–95 km depth (stations used: N.YMZF, N.ONSF, N.JIZF)
- R0100: 140.8–143.2E, 37.8–40.2N, 5–95 km depth (stations used: N.TMRF, N.GJMF, N.KSKF)

### 3.2. Green's functions and moment tensors

For computation of the Green's function, eight-component seismograms are computed in advance, namely  $T_{SS}$ ,  $T_{DS}$ ,  $R_{SS}$ ,  $R_{DS}$ ,  $R_{DD}$ ,  $Z_{SS}$ ,  $Z_{DS}$ , and  $Z_{DD}$  (for the notation of these terms, see Herrmann and Wang, 1985), for depths at every 9 km from 5 to 95 km and for epicentral distances at every 5 km from 30 to 500 km, covering the first 300 s from the origin time (which is counted as 0 s). We use Saikia's (Saikia, 1994) frequency wave number integration method. The obtained components were then saved onto a disk. The velocity structure used to compute the Green's function is the same as the one used by the Japanese F-net moment tensor inversion (Fukuyama et al., 1998) as listed Table 1.

The current GRiD MT solves only for the deviatoric components of a moment tensor, and the 8-component synthetic seismograms stored on the disk are converted to Green's functions corresponding to the 5 deviatoric components which are stored in the memory.

## 4. Results and performance

GRiD MT has been monitoring the area R0010 starting from April, 2003, Fig. 4 shows the monitoring results obtained from January 2004 to December 2006. In all, 550 earthquakes are detected, including some overlaps. Table 2 lists the determined source parameters of selected events with moment magnitude larger than 5.0, and Fig. 5 shows an example for an earthquake,  $M_w = 6.2$ .

### 4.1. Comparison with JMA catalog

As GRiD MT does not rely upon a preliminary report of the earthquake information, it is important to check the location and origin time with catalogues determined by dense short-period seismic networks. We compare GRiD MT results with the earthquake catalog data provided by the Japan Meteorological Agency (JMA). Fig. 6 shows the differences between the locations obtained by GRiD MT and those derived from the JMA catalogue. The horizontal grid size for the virtual sources is  $0.1^\circ$ , and the results show horizontal differences that are generally less than two grids (averaged differences and standard deviations are  $19.4 \pm 11.9$  km). There appears to be a systematic bias in the estimate of the epicentral longitude; earthquakes are located further offshore. We attribute this to the inadequacy of the used structural model. The seismic velocity in the frontal arc region is likely to be slower than the main island arc part. The usage of a faster reference model should result in mislocation further offshore. The vertical (depth) differences are also

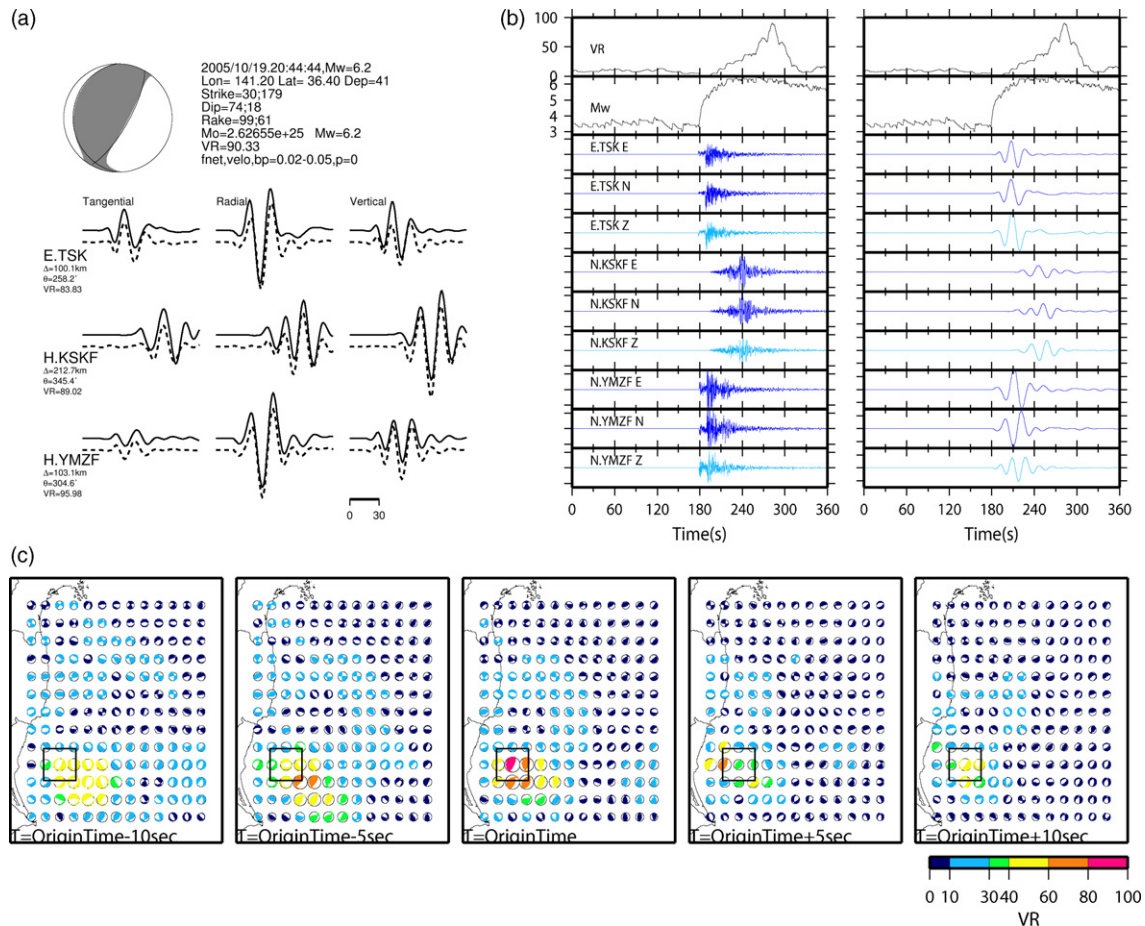


**Fig. 5.** Example of the monitoring result for an earthquake 2005/Oct/19 20:44:44  $M_w = 6.2$ . (a) The focal mechanism determined by GRiD MT. The solid lines and dashed lines represent the observed and synthetic waveforms, respectively. (b) Monitoring outputs of variance reduction and magnitude ( $=M_w$ ). Raw waveforms (left) and waveforms filtered in the 20–50 mHz band (right). (c) Snap shots of moment tensors and variance reduction. Time in each window are listed in the left bottom. Box shows the best source location. The size of focal mechanism are scaled by  $M_w \times (0.5 + 0.5 \times (VR/100))$ .

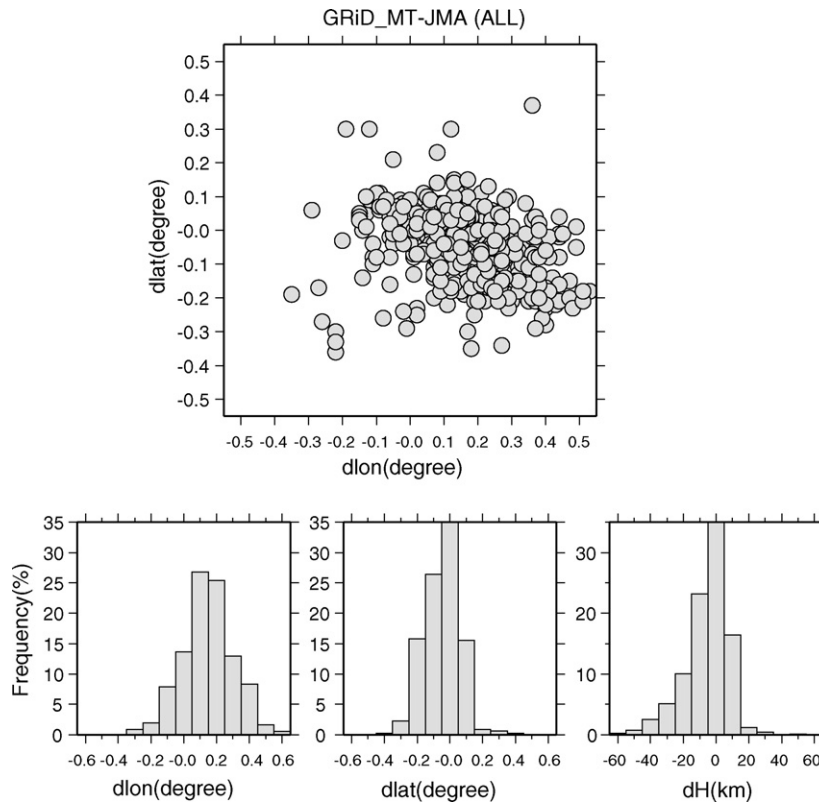


**Fig. 6.** Horizontal and depth differences of the GRiD MT locations and the Japan Meteorological Agency (JMA) catalogues. The difference pairs of longitude and latitude are plotted (top). There appears a systematic bias in the longitude difference. Histogram of the longitude difference (bottom left), latitude difference (bottom center) and depth difference (bottom right).

within two vertical grid points. The usage of a more appropriate structural model or a 3-D model would reduce these mislocations.

Fig. 7 shows differences of origin time of GRiD MT and JMA catalogue. The differences of origin times are 3 s or less (averaged differences and standard deviations are  $-0.3 \pm 3.2$  s). As GRiD MT

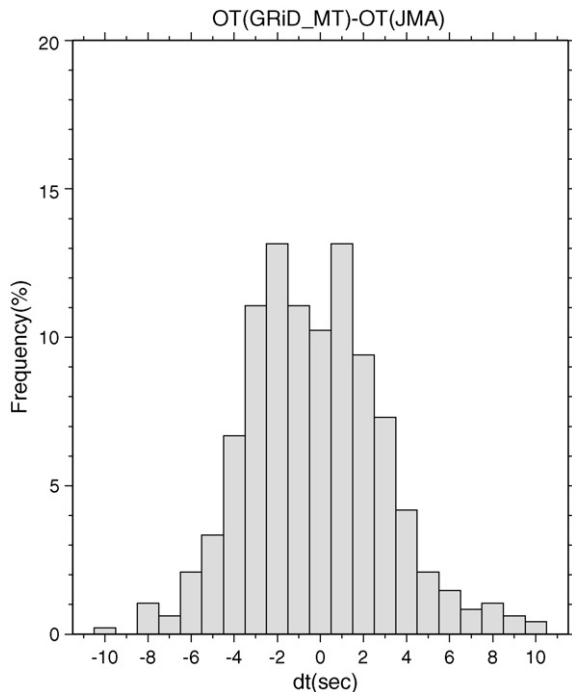


**Fig. 7.** Origin time of differences of GRiD MT and JMA catalogues.

is performed in a frequency band of 20–50 s, these results are considered to be of high precision.

Fig. 8 compares computed magnitudes with those from the catalogue data. Although both are in agreement in general, differences and variations are greater and scattered for smaller earthquakes. The maximum differences in magnitude between the two methods are 0.6 (averaged differences and standard deviations are  $0.00 \pm 0.27$ ). It is well known that the magnitude estimated by JMA tend to be larger than the corresponding moment magnitudes for large earthquakes (Takemura, 1990). Although the average difference is 0.00, for relatively large events ( $M_j > 4.5$ ),  $M_j$  is about 0.1 larger on the average than  $M_w$  of GRiD MT.

All in all, we conclude that GRiD MT obtains origin time and locations with a high level of precision both in time and space.

#### 4.2. Comparison with F-net solutions

The broadband seismic network F-net operated by the National Research Institute for Earth Science and Disaster Prevention (NIED) provided on line their moment tensor solutions. Although the F-net solutions assume a preliminary epicenter provided by JMA, they do estimate the depth of earthquakes. We compare GRiD MT solutions with the manually determined F-net solutions available on the Internet. Fig. 9 shows a comparison of the obtained moment magnitudes. The magnitudes obtained by the two methods have differences of approximately 0.1 or less (averaged differences and standard deviations are  $0.03 \pm 0.08$ ), and are very similar. Differences in depth estimated by the two methods are shown in Fig. 10; again the similarity is strong, with differences being less than 2 vertical grid points. With respect to depth, the R0010 and R0100 monitoring areas results tend to be shallower than the corresponding F-net results. We attribute this trend to the fact that F-net solutions use the assumed epicenters obtained by JMA.

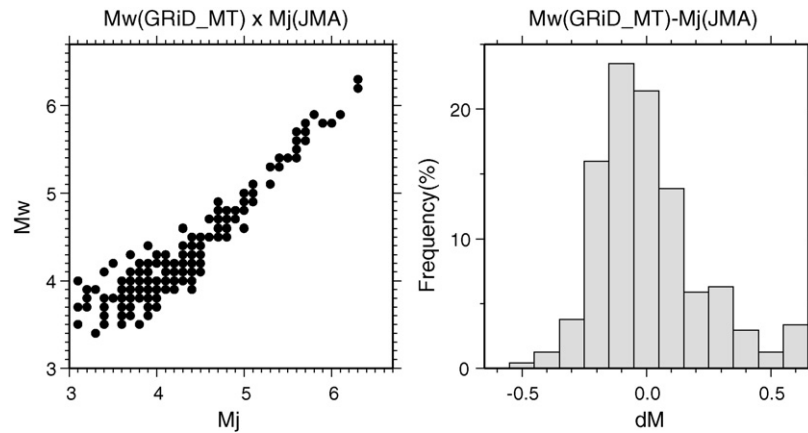


Fig. 8. Correlation of the magnitude of GRiD MT and JMA catalogues (left). Histogram of the difference in magnitude by GRiD MT and JMA catalogues (right).

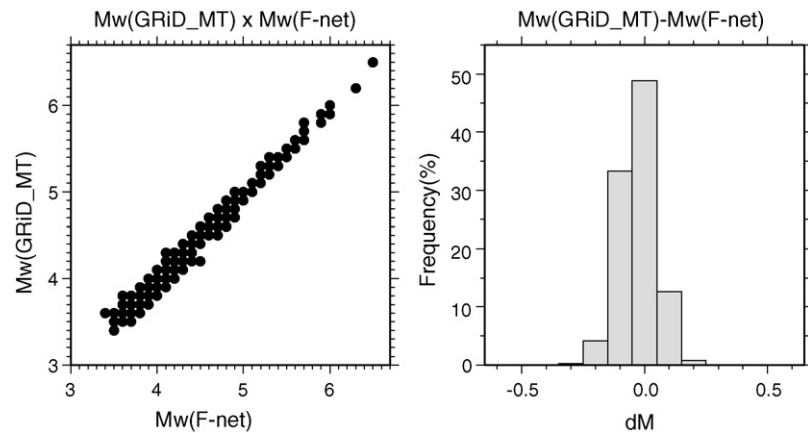


Fig. 9. Correlation of the moment magnitude of GRiD MT and F-net catalogues by NIED (left). Histogram of the difference in moment magnitude by GRiD MT and F-net catalogues (right).

We next compare earthquake mechanisms. In comparing mechanism solutions, we use an index of similarity of two moment tensors introduced by Kuge and Kawakatsu (1993). This index is the cross-correlation of P-wave radiation patterns. The index value is 1

if the two mechanisms are identical, and  $-1$  if they are completely different. The index value is not affected by the size of the earthquake. The comparison results are shown in Fig. 11. The similarity is 0.8 or higher for most of the data, indicating that the obtained mechanisms are very similar.

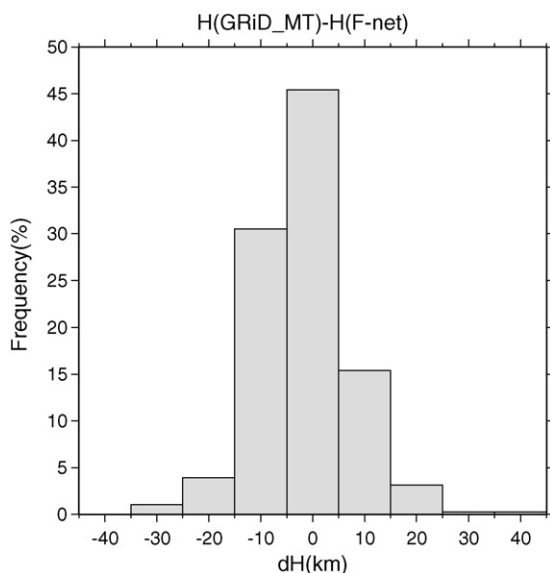
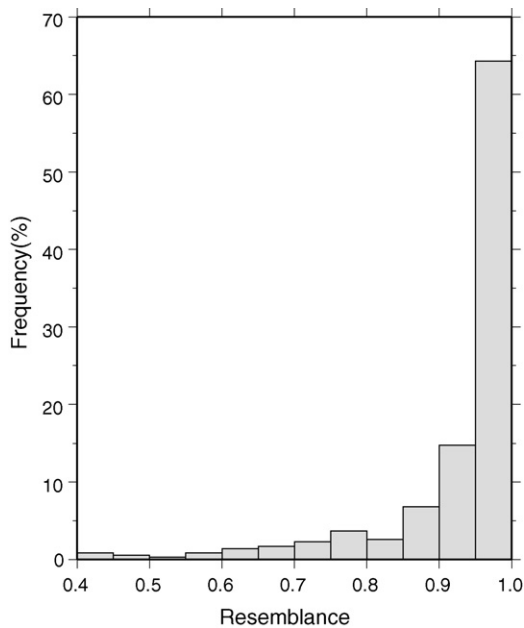


Fig. 10. Histogram of the depth differences of GRiD MT and F-net catalogues.

#### 4.3. Threshold of the VR

The VR threshold is set at  $VR=65.0$  for this study. This setting enables the detection of earthquakes with a magnitude of larger than approximately 4.5, as defined by JMA magnitude (note that  $M_j$  is larger than  $M_w$  by about 0.2). To detect smaller earthquakes, we need to lower the threshold value; however, a lower threshold value results in more false detections. Fig. 12 shows the relation between VR threshold and false alarm rate. With the VR threshold at 65.0, 26.4% of the detected cases by GRiD MT are false detections. We have examined the possibility that some of these events are actually real “unusual” events, but could not identify any. The presence of unusual (e.g., very-low-frequency) earthquakes are not established along the Pacific coast of northeastern Japan.

Although a larger VR threshold reduces the number of false detections, it also results in the fewer earthquakes detections. Also VR can become as high as 50 due to teleseismic earthquakes. To detect as many earthquakes as possible while reducing the number of false detections, GRiD MT might need to cooperate with short-period signals. The use of a larger number of stations might solve this problem of teleseismic events.



**Fig. 11.** Histogram of the mechanism resemblance of GRiD MT and F-net catalogues. Resemblance is the cross-correlation of P-wave radiation patterns. The index value is 1 if the two mechanisms are identical, and  $-1$  if they are completely different.

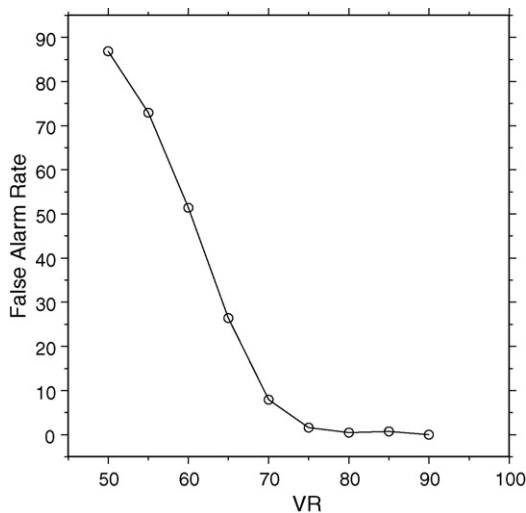


**Fig. 12.** Probability that a signal is a false earthquake. With the VR threshold at 65.0, 26.4% of the detected cases are false detections.

In Fig. 13, the vertical axis indicates the ratio of total number of earthquakes (with magnitudes  $\geq M$ ) determined by JMA to that detected by GRiD MT, and the horizontal axis refers to the JMA magnitude. The three lines show cases that correspond to three different VR thresholds, 50 ( $\Delta$ ), 65 (o), and 70 (+). With the threshold set at 65, the value chosen for our monitoring, GRiD MT detects 90% of earthquakes with magnitude  $\geq 4.5$ . For the remaining 10% of events, the long-period wavefield was found to be contaminated by surface waves of large teleseismic earthquakes. Detection rate decreased for earthquakes with magnitude larger than 6.

## 5. Discussion

We established a functioning streaming moment tensor method that works well with our initial definition of operating parameters. However, there are areas that can be improved, and which

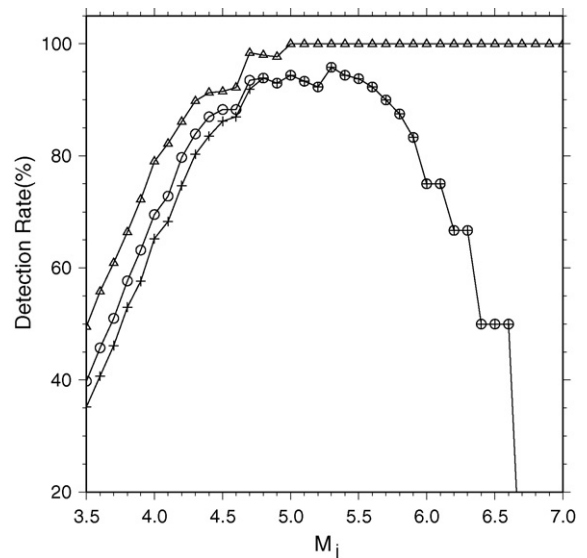


**Fig. 13.** Detection rate of events for JMA catalogue. The vertical axis indicates the ratio of total number of earthquakes with magnitudes  $\geq M$  determined by JMA to that detected by GRiD MT, and the horizontal axis refers to the JMA magnitude. The three lines show cases that correspond to three different VR thresholds, 50 ( $\Delta$ ), 65 (o), and 70 (+).

are the focus of future works such as how to deal with missing data, establishing multiple distributed PC processing, adjusting the monitoring period range to account for larger earthquakes, and for specialized monitoring of long-period events.

In terms of missing data, the most important problem to consider at this point is how to deal with missing waveform data. In such a case, our system is unable to correctly detect an earthquake. As this problem arises from the fact that data is currently being used from three fixed stations, we need to consider building and employing a new algorithm that monitors three stations out of more where data is collected.

In terms of Multiple-PC processing, to expand the coverage area (e.g., entire Japan), multiple PCs will be needed in distributed processing. The analysis results from all PCs would then need to be integrated effectively and correctly. In the present study, two or more different monitoring areas partially overlap each other, and multiple sets of information are detected for same earthquakes. This overlapping of information must be avoided.

In terms of monitoring period range, the current system is more-or-less successful in monitoring the period range of 20–50 s. The system may not be able to properly detect an earthquake larger in size, as the assumption of a point source does not hold true for such a large earthquake. The monitoring period range would need to be adjusted depending on actual monitoring purposes. For larger earthquakes, it will be necessary to use longer period and far station data (Fukuyama and Dreger, 2000).

In terms of monitoring “long-period” events, seismology has now experienced plenty examples of “long-period” seismic events (e.g., Kanamori and Given, 1982; Kawakatsu et al., 1994; Ekström et al., 2003) which may not be detected using conventional monitoring of short-period seismic networks. Recently, Ito et al. (2007) added new such an example by employing a grid-based approach to discover ultra-low frequency earthquakes in the deeper portion of the seismogenic zone beneath southwest Japan, where major interplate earthquakes are expected in the near future. With GRiD MT monitoring a long-period wavefield, such “long-period” events can be also regularly monitored. Although in our current system, the isotropic moment tensor and the single force component are not monitored, such inclusion is possible and is planned in the

near future which should further expand our ability to detect ‘long-period’ events in real-time.

## 6. Conclusions

The GRiD MT described in this paper utilizes real-time broadband seismic waveform records collected and distributed by a satellite or terrestrial telemetry system. It continuously monitors long-period wavefields of 20–50 s period to automatically determine earthquake origin times and locations as well as mechanisms (moment tensor solutions). GRiD MT is the first of its kind in the world, and after three years of monitoring we reached the following conclusions: (1) GRiD MT detects earthquakes and determines the source parameters with a high level of precision and complete automation within 3 min of the earthquake occurrence. (2) The origin time and locations obtained using our system are very similar to those of JMA catalogue. (3) The mechanism and moment magnitude obtained by our system are very similar to the corresponding F-net solutions determined by NIED.

The above conclusions suggest that GRiD MT can be highly effective in the further development of new seismic analysis systems that are able to monitor long-period earthquakes that none of the conventional short-period wavefield monitoring systems are able to detect. Our monitoring results also prove the feasibility of continuously monitoring of the long-period seismic wavefield. Incorporation of more accurate structural models (e.g., 3-D), and/or the usage of different period data, should result in more accurate description of the earthquake activity field in real-time.

## Acknowledgments

We thank Prof. Doug Dreger and an anonymous reviewer who provided helpful review comments that substantially improved the manuscript. We used the F-net data provided by the National Research Institute for Earth Science and Disaster Prevention. We also used FKRPROG, developed by Saikia, for the computation of the Green’s function.

## References

- Auger, E., D’Auria, L., Martini, M., Chouet, B., Dawson, P., 2006. Real-time monitoring and massive inversion of source parameters of very long period seismic signals: an application to Stromboli Volcano, Italy. *Geophys. Res. Lett.*, L04301.
- Bernardi, F., Braunmiller, J., Kradolfer, U., Giardini, D., 2004. Automatic regional moment tensor inversion in the European-Mediterranean region. *Geophys. J. Int.*, 703–716.
- Dreger, D., Helmberger, D.V., 1993. Determination of source parameters at regional distances with single station or sparse network data. *J. Geophys. Res.*, 8107–8125.
- Dziewonski, A.M., Chou, T.-A., Woodhouse, J.H., 1981. Determination of earthquake source parameters from waveform data for studies of global and regional seismicity. *J. Geophys. Res.*, 2825–2852.
- Ekström, G., Nettles, M., Abers, G.A., 2003. Glacial earthquakes. *Science*, 622–624.
- Fukuyama, E., Ishida, M., Dreger, D.S., Kawai, H., 1998. Automated seismic moment tensor determination by using on-line broadband seismic waveforms. *Zisin*, 149–156 (in Japanese with English abstract).
- Fukuyama, E., Dreger, D.S., 2000. Performance test of an automated moment tensor determination system for the future ‘‘Tokai’’ earthquake. *Earth Planets Space*, 383–392.
- Herrmann, R.B., Wang, C.Y., 1985. A comparison of synthetic seismograms. *Bull. Seism. Soc. Am.*, 41–56.
- Ito, Y., et al., 2006. Performance of regional distance centroid moment tensor inversion applied to the 2004 mid-Niigata prefecture earthquake, Japan. *Geophys. J. Int.*, 1317–1331.
- Ito, Y., et al., 2007. Slow earthquakes coincident with episodic tremors and slow slip events. *Science*, 503–506.
- Kanamori, H., Given, J.W., 1982. Analysis of long-period seismic waves excited by the May 18 1980 eruption of Mount St. Helens—a terrestrial monopole. *J. Geophys. Res.*, 5422–5432.
- Kanamori, H., Maechling, P., Hauksson, E., 1999. Continuous monitoring of ground-motion parameters. *Bull. Seism. Soc. Am.*, 311–316.
- Kawakatsu, H., Ohminato, T., Ito, H., 1994. 10s-period volcanic tremors observed over a wide area in southwestern Japan. *Geophys. Res. Lett.*, 1963–1966.
- Kawakatsu, H., 1995. Automated near-realtime CMT inversions. *Geophys. Res. Lett.*, 2569–2572.
- Kawakatsu, H., 1998. On the realtime monitoring of the long-period seismic wavefield. *Bull. Earthquake Res. Inst.*, 267–274.
- Kuge, K., Kawakatsu, H., 1993. Significance of non-double couple components of deep and intermediate-depth earthquakes: implications from moment tensor inversions of long-period seismic waves. *Phys. Earth Planet. Inter.*, 243–266.
- Saikia, C.K., 1994. Modified frequency-wave number algorithm for regional seismograms using Filon’s quadrature, modeling of Lg waves in eastern North America. *Geophys. J. Int.*, 142–158.
- Saito, M., 1978. An automatic design algorithm for band selective recursive digital filters. *Geophys. Exploration*, 240–263.
- Sipkin, S., 1994. Rapid determination of global moment-tensor solutions. *Geophys. Res. Lett.*, 1667–1670.
- Tajima, F., Megnin, C., Dreger, D.S., Romanowicz, B., 2002. Feasibility of real-time broadband waveform inversions for simultaneous moment tensor and centroid location determination. *Bull. Seism. Soc. Am.*, 739–750.
- Takemura, M., 1990. Magnitude-seismic moment relations for the shallow earthquakes in and around Japan. *Zisin*, 257–265 (in Japanese with English abstract).
- Takano, T., Taku, U., Hirata, N., Kasahara, K., Obara, K., Hori, S., Nishide, N., Wakayama, M., Nakazawa, H., Matsumori, T., 2001. Development of the national real-time distribution system of high sensitivity waveform data program and abstracts. *Seism. Soc. Jpn.* 2, B57.
- Thio, K.H., Kanamori, H., 1995. Moment tensor inversion for local earthquakes using surface waves recorded at TERRAscope. *Bull. Seism. Soc. Am.*, 1021–1038.
- Urabe, T., 1994. A common format for multi-channel earthquake waveform data program and abstracts. *Seism. Soc. Jpn.* 2, P24.